

The XMM-Newton Needles in the Haystack Survey: the local X-ray luminosity function of ‘normal’ galaxies

I. Georgantopoulos¹, A. Georgakakis¹, E. Koulouridis^{1,2}

¹ Institute of Astronomy & Astrophysics, National Observatory of Athens, I. Metaxa & V. Pavlou, Athens, 15236, Greece

² Astronomical Laboratory, Department of Physics, University of Patras, 26500 Rio-Patras, Greece

11 June 2021

ABSTRACT

In this paper we estimate the local ($z < 0.22$) X-ray luminosity function of ‘normal’ galaxies derived from the *XMM-Newton* Needles in the Haystack Survey. This is an on-going project that aims to identify X-ray selected ‘normal’ galaxies (i.e. non-AGN dominated) in the local Universe. We are using a total of 70 *XMM-Newton* fields covering an area of 11 deg² which overlap with the Sloan Digital Sky Survey Data Release-2. ‘Normal’ galaxies are selected on the basis of their resolved optical light profile, their low X-ray-to-optical flux ratio ($\log(f_x/f_o) < -2$) and soft X-ray colours. We find a total of 28 candidate ‘normal’ galaxies to the 0.5–8 keV band flux limit of $\approx 2 \times 10^{-15}$ erg cm⁻² s⁻¹. Optical spectra are available for most sources in our sample (82 per cent). These provide additional evidence that our sources are bona-fide ‘normal’ galaxies with X-ray emission coming from diffuse hot gas emission and/or X-ray binaries rather than a supermassive black hole. Sixteen of our galaxies have narrow emission lines or a late-type Spectral Energy Distribution (SED) while the remaining 12 present only absorption lines or an early-type SED. Combining our *XMM-Newton* sample with 18 local ($z < 0.22$) galaxies from the *Chandra* Deep Field North and South surveys, we construct the local X-ray luminosity function of ‘normal’ galaxies. This can be represented with a Schechter form with a break at $L_* \approx 3_{-1.0}^{+1.4} \times 10^{41}$ erg s⁻¹ and a slope of $\alpha \approx 1.78 \pm 0.12$. Using this luminosity function and assuming pure luminosity evolution of the form $\propto (1+z)^{3.3}$ we estimate a contribution to the X-ray background from ‘normal’ galaxies of $\sim 10\text{--}20$ per cent (0.5–8 keV). Finally, we derive, for the first time, the luminosity functions for early and late type systems separately.

Key words: Surveys – X-rays: galaxies – X-rays: general – galaxies: luminosity function

1 INTRODUCTION

In the last decade, ‘normal’ galaxies (i.e. non-AGN dominated) have been studied in detail at X-ray wavelengths by various missions through observations of optically selected systems (e.g. Fabbiano, Kim & Trinchieri 1992; Read, Strickland & Ponman 1997; Kilgard et al. 2002). The X-ray emission in these systems appears to come from diffuse hot gas and/or X-ray binaries. In the most massive early-type systems the X-ray emission is dominated by the hot interstellar medium having temperatures of about 1 keV. Low mass X-ray binaries associated with the older stellar population are responsible for a smaller fraction of the observed X-ray luminosity. In late-type systems, the X-ray emission originates in both hot gas with temperature of about $kT \sim 1$ keV (heated by supernova remnants), as well as a mixture of low and high

mass X-ray binaries (for a review see Fabbiano 1989). The diffuse hot gas contributes significantly in the soft X-ray band (<2 keV) while the X-ray binary systems are responsible for the bulk of the emission at harder energies (e.g. Stevens, Read & Bravo-Guerrero 2003). In general, the integrated X-ray emission of ‘normal’ galaxies is believed to be a good indicator of the star-formation activity in these systems (e.g. Gilfanov, Grimm & Sunyaev 2004).

The X-ray luminosity of ‘normal’ galaxies is usually weak, $\lesssim 10^{42}$ erg s⁻¹ a few orders of magnitude below that of powerful AGNs, resulting in faint observed X-ray fluxes. As a consequence, until recently, only the very local systems (< 100 Mpc) had been accessible to X-ray missions leaving the issue of galaxy evolution at X-ray wavelengths open. This has completely changed with the new generation X-ray

missions, the *Chandra* and the *XMM-Newton*. The *Chandra* Deep Fields (CDF; Alexander et al. 2003; Giacconi et al. 2002) reaching fluxes $f(0.5-2 \text{ keV}) < 10^{-16} \text{ erg s}^{-1} \text{ cm}^{-2}$ have indeed, provided the first ever X-ray selected ‘normal’ galaxy sample. In a pioneering work, Hornschemeier et al. (2003) used the 2 Ms CDF-North to provide a sample of 43 ‘normal’ galaxy candidates with available optical spectroscopy. Norman et al. (2004) extended this study and identified over 100 ‘normal’ galaxy candidates in the combined CDF-North and South albeit with optical spectroscopy limited to a fraction of them. Both these studies find distant galaxies ($z < 1$) at a median redshift of $z \approx 0.3$.

Despite the great progress in the field achieved by *Chandra*, there is a pressing need for a local X-ray selected ‘normal’ galaxy sample to complement the deeper CDF studies and to provide the X-ray luminosity function of these systems in the nearby Universe. Motivated by this we initiated a project using *XMM-Newton* aiming to identify X-ray selected ‘normal’ galaxies at bright fluxes. The large field-of-view combined with the high effective area of *XMM-Newton* make this mission ideal for this study. Our fields are selected to overlap with the Sloan Digital Sky Survey (SDSS), Data Release-2 to exploit the good quality and homogeneous five-band optical photometry and optical spectroscopy. First results from this on-going survey have been reported in Georgakakis et al. (2004b). Similar studies have been recently performed with the HRI detector onboard *ROSAT* (Tajer et al. 2005). Our main goal in this paper is to expand the Georgakakis et al. (2004b) sample to determine the X-ray galaxy luminosity function in the local Universe, $z \lesssim 0.2$. Throughout this paper we adopt $H_0 = 70 \text{ km s}^{-1} \text{ Mpc}^{-1}$, $\Omega_M = 0.3$ and $\Omega_\Lambda = 0.7$.

2 THE DATA ACQUISITION

2.1 The *XMM-Newton* Observations

In this paper we use *XMM-Newton* archival observations, with a proprietary period that expired before June 2004, that overlap with second data release of the SDSS (DR2; Stoughton et al. 2002). Only observations that use the EPIC (European Photon Imaging Camera; Strüder et al. 2001; Turner et al. 2001) cameras as the prime instrument operated in full frame mode were employed. We use only fields at high Galactic latitude $|b| > 20^\circ$ in order to minimize the absorption as well as the stellar contamination. We also reject fields which contain bright clusters as their target. Finally, fields that are heavily contaminated by high particle background periods are excluded from the analysis. For fields observed more than once with the *XMM-Newton* we use the deeper of the multiple observations. A total of 42 new fields are used in addition to the 28 *XMM-Newton* observations used in Georgakakis et al. (2004b). Details of all 70 fields are given in Table 1.

We are using the Pipeline Processing Subsystem (PPS) event files. The event files were screened for high particle background periods by rejecting times with 0.2-10 keV count rates higher than 25 and 15 cts/s for the PN and the two MOS cameras respectively. The resulting PN and MOS exposures are shown in Table 1. The differences between the PN and MOS exposure times are due to varying start

and end times of individual observations. Only events corresponding to patterns 0–4 for the PN and 0–12 for two MOS cameras have been kept. To increase the signal-to-noise ratio and to reach fainter fluxes the PN and the MOS event files, where available, have been combined into a single event list using the MERGE task of SAS. Images in celestial coordinates with pixel size of 4.35 arcsec have been extracted in the spectral bands 0.5–2 keV (soft) and 2–8 keV (hard) for the merged event file. Exposure maps accounting for vignetting, CCD gaps and bad pixels have been constructed for each spectral band. We apply no astrometric corrections in our data. However, we estimate the astrometric accuracy of the *XMM-Newton* positions to be better than 3 arcsec (see section 3). Source detection is performed in the 0.5–8 keV merged PN+MOS images using the EWAVELET task of SAS with a detection threshold of 5σ . Count rates in the merged (PN+MOS) images as well as the individual PN and MOS images are estimated within an 18 arcsec aperture. For the background estimation we use the background maps generated as a by-product of the EWAVELET task of SAS. The merged image count rates are used for flux estimation, while the individual PN or MOS count rates are used for hardness ratios. This is because the interpretation of hardness ratios is simplified if the extracted count rates are from one detector only. A small fraction of sources lie close to masked regions (CCD gaps or hot pixels) on either the MOS or the PN detectors. This may introduce errors in the estimated source counts. To avoid this bias, the source count rates (and hence the hardness ratios and the flux) are estimated using the detector (MOS or PN) with no masked pixels in the vicinity of the source. We define the hardness ratio as $HR = H-S/H+S$, where H and S are the source count rates in the 2–8 keV and 0.5–2 keV band respectively. Hence, a more negative hardness ratio value, suggests a softer (steeper) X-ray spectrum. To convert counts to flux the Energy Conversion Factors (ECF) of individual detectors are calculated assuming a power law spectrum with $\Gamma = 1.8$ and Galactic absorption appropriate for each field (Dickey & Lockman 1990). We do not apply any correction for Galactic absorption. However, for the median Galactic column density of our ‘normal’ galaxy sample ($N_H \approx 2.8 \times 10^{20} \text{ cm}^{-2}$) such a correction is small, only about 4 per cent of the 0.5–8 keV flux.

Next, we derive the area curve i.e. the solid angle as a function of the 5σ limiting flux for our observations. For each pixel of the background map, generated as a by product of the EWAVELET task, we estimate the 5σ background fluctuations. We then scale to the area of a circular aperture with a size of 4 pixel radius. The 4 pixel scale encircles 70 per cent of the light (at an energy of 1.5 keV) and roughly corresponds to the scale of the wavelet filter used for detection. These values are then divided with the corresponding exposure time and are converted to flux. The area curve is derived using the merged PN and MOS background and exposure maps where available or the single PN and MOS maps. We have checked that the area curve derived above gives reasonable results by estimating the 0.5–8 keV $\log N - \log S$ for all the X-ray sources in our fields and comparing with the number counts derived from other surveys (e.g. Manners et al. 2003). Figure 1 shows the solid angle covered by our survey as a function of the 0.5–8 keV limiting flux.

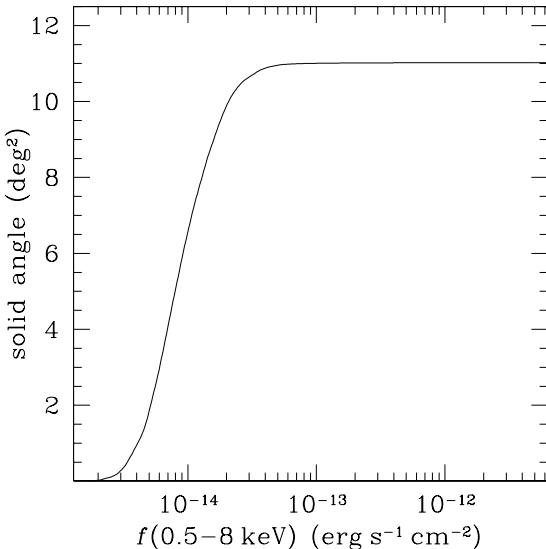


Figure 1. Solid angle as a function of limiting flux (5σ) in the total 0.5–8 keV band for our survey.

2.2 The SDSS data

The SDSS is an ongoing imaging and spectroscopic survey which has covered so far (DR-2) $\approx 3324 \text{ deg}^2$ of the sky. Photometry is performed in 5 bands ($ugriz$; Fukugita et al. 1996; Stoughton et al. 2002) to the limiting magnitude $g \approx 23$ mag, providing a uniform and homogeneous multi-color photometric catalogue. The SDSS spectroscopic observations obtain spectra of galaxies brighter than $r = 17.7$ mag as well as of luminous red galaxies with $r < 19.2$ mag (York et al. 2000; Stoughton et al. 2002).

We identify the optical counterparts of the X-ray sources following the method of Downes et al. (1986) to calculate the probability, P , that a given candidate is the true identification. We apply an upper limit in the search radius, $r < 7 \text{ arcsec}$ and a cutoff in the probability, $P < 0.05$, to limit the optical identifications to those candidates that are least likely to be chance coincidences.

3 GALAXY SELECTION

‘Normal’ galaxy candidates are selected to have (i) extended optical light profile, i.e. resolved (see Stoughton et al. 2002), to avoid contamination of the sample by Galactic stars, (ii) X-ray-to-optical flux ratio $\log(f_x/f_o) < -2$, two orders of magnitude lower than typical AGNs. The $\log f_x/f_o$ is estimated from the relation

$$\log \frac{f_x}{f_o} = \log f_x(0.5 - 8 \text{ keV}) + 0.4 r + 5.39. \quad (1)$$

The equation above is derived from the X-ray-to-optical flux ratio definition of Stocke et al. (1991) that involved 0.3–3.5 keV flux and V -band magnitude. These quantities are converted to 0.5–8 keV flux and r -band magnitude assuming a mean colour $V - R = 0.7$ and a power-law X-ray spectral energy distribution with index $\Gamma = 1.8$. The sample of ‘normal’ galaxy candidates is presented in Table 2. We further exclude from the sample sources with hard X-ray colours

(hardness ratio $HR > 0$) roughly corresponding to a spectrum with a hydrogen column density higher than 10^{22} cm^{-2} (assuming a power-law index of $\Gamma = 1.9$). The three hard sources (#7, 15, 28) are most likely associated with low luminosity obscured AGN. These are presented in Table 3. Note however, that for a few sources (#08, 10, 14, 29) we do not have enough photon statistics to place a stringent constraint on their X-ray spectrum. We also exploit the SDSS optical spectroscopic information available for our sources to search for AGN signatures using emission line ratios. Sixteen of our galaxies have either a narrow emission line optical spectrum or a Spectral Energy Distribution (SED), as derived from the SDSS colours, consistent with a late-type spectrum. Twelve galaxies either present only absorption lines or their SED is consistent with an early-type spectrum. We employ the CMU-PITT SDSS Value Added Database (VAC database^{*}) which provides spectral classifications for the SDSS galaxies using diagnostic emission line ratios ($[\text{N II}]/\text{H}\alpha$, $[\text{O III}]/\text{H}\beta$, $[\text{S II}]/\text{H}\alpha$, $[\text{O I}]/\text{H}\alpha$; Miller et al. 2003). All emission line systems in Table 2 with available spectroscopic classifications have emission-line ratios consistent with star formation activity. However, we note that a number of sources with both absorption (e.g. $\text{H}\beta$) and emission-line optical spectra have uncertain classification based on one line ratio only, usually $[\text{N II}]/\text{H}\alpha$. These are marked in Table 2.

The archival X-ray data used here include targeted observations of nearby normal galaxies with low X-ray-to-optical flux ratio. Such sources have been excluded from Table 2. Moreover, a number of ‘normal’ galaxy candidates although not the prime target of the *XMM-Newton* pointing lie at the same redshift as the prime target and are therefore most likely directly associated with it (e.g. cluster or group members). These sources are marked in Table 2. The final sample of ‘normal’ galaxy candidates that are not showing evidence for AGN activity comprises 28 sources. Of these only five do not have optical spectroscopy available. Although no astrometric corrections have been applied to our data the positional accuracy of *XMM-Newton* is sufficient for the purpose of this paper. We quantify the astrometric accuracy of the *XMM-Newton* by constructing the distribution of the X-ray/optical position angular offset for all the X-ray sources detected in our survey with an optical counterpart. This is well described by a Gaussian distribution with 1σ rms of 1.7 arcsec for the bright X-ray sources (>75 counts) and 2.8 arcsec for the fainter ones (<75 counts). In Table 2 the offset between the optical and X-ray coordinates for our 28 galaxies is $\lesssim 5$ arcsec, within the 2σ positional uncertainty for faint sources derived above.

4 THE LUMINOSITY FUNCTION

The luminosity-redshift relation for our sample is compared in Fig. 2 with the ‘normal’ galaxies from the CDF-North and South. For the CDF-North we use the spectroscopic sample of Hornschemeier et al. (2003) while for the CDF-South we select $\log(f_x/f_o) < -2$ sources from the 0.5–2 keV catalogue of Giacconi et al. (2002) with spectroscopic or photometric redshifts obtained from Szokoly et al. (2004) and Zheng et

^{*} [HTTP://ASTROPHYSICS.PHYS.CMU.EDU/DR3/](http://ASTROPHYSICS.PHYS.CMU.EDU/DR3/)

Obs ID	RA (J2000)	Dec (J2000)	FILTER	N_{H} (10^{20} cm^{-2})	PN exp. time (ksec)	MOS1 exp. time (ksec)	Field name
0065140101	00 42 31	-09 41 29	MEDIUM	3.60	9.0	12.4	ABELL85
0090070201	00 43 20	-00 51 15	MEDIUM	2.33	15.7	—	UM 269
0093641001	01 43 02	+13 38 30	MEDIUM	4.87	6.3	11.0	NGC 660
0084230401	01 52 42	+01 00 43	MEDIUM	2.80	5.8	17.2	ABELL 267
0101640201	01 59 50	-00 23 41	MEDIUM	2.65	3.8	—	MRK 1014
0093630101	02 41 05	-08 15 21	MEDIUM	3.07	12.3	15.6	NGC 1052
0056020301	02 56 33	-00 06 12	THIN	6.50	—	11.6	RX J0256.5+0006
0041170101	03 02 39	-00 07 40	THIN	7.16	38.1	46.9	CFRS 3H
0142610101	03 06 41	+00 01 12	THIN	6.96	33.5	45.8	S2F1A
0103861001	03 25 25	-06 08 30	MEDIUM	4.39	6.8	—	MRK609
0134540601	03 36 47	+00 35 15	MEDIUM	8.17	30.3	35.1	HR1099
0036340101	03 38 29	+00 21 56	THIN	8.15	8.9	6.7	SDSS 033829.31+00215
0094790201	03 57 22	+01 10 56	THIN	13.20	19.1	21.4	HAWAII 167
0152530101	08 10 57	+28 08 33	THIN	3.73	16.7	22.1	YZ CNC
0092800201	08 31 41	+52 45 18	MEDIUM	3.83	66.8	73.3	APM 08279+5255
0111971701	08 38 22	+48 38 01	MEDIUM	3.41	7.2	—	EI UMA
0103660201	08 47 42	+34 45 05	MEDIUM	3.28	13.0	—	PG 0844+349
0085150301	08 49 18	+44 49 24	MEDIUM	2.63	29.3	35.1	LYNX 3A-SE
0083240201	09 11 27	+05 50 52	THIN	3.67	—	17.7	RX J0911.4
0084230601	09 17 53	+51 43 38	MEDIUM	1.44	15.9	13.6	ABELL 773
0112520201	09 34 02	+55 14 20	THIN	1.98	23.5	28.5	IZW 18
0085640201	09 35 51	+61 21 11	THIN	2.70	20.4	33.9	UGC 5051
0106460101	09 43 00	+46 59 30	THIN	1.24	—	46.5	CL0939+472
0070940401	09 53 41	+01 34 46	THIN	3.46	—	12.9	NGC3044
0070340201	10 08 48	+53 42 03	THIN	7.57	18.0	20.8	WJ1008.7
0108670101	10 23 40	+04 11 24	THIN	2.94	45.6	52.6	ZW 3146
0147511701	10 52 41	+57 28 29	MEDIUM	5.58	84.1	95.5	LOCKMAN HOLE
0083000301	11 23 09	+05 30 19	MEDIUM	4.39	23.3	28.2	3C 257
0112810101	11 28 30	+58 33 43	THIN	9.92	13.8	20.0	NGC 3690
0111970701	11 38 27	+03 22 07	MEDIUM	2.36	9.0	—	T LEO
0094800201	11 40 23	+66 08 41	THIN	1.18	19.0	24.7	MS1137.5
0044740201	11 50 42	+01 45 53	THICK	2.22	41.3	47.9	BETA VIR
0049340301	11 51 07	+55 04 45	MEDIUM	1.14	20.3	25.0	NGC 3921
0090020101	11 57 56	+55 27 12	THIN	1.22	8.0	11.1	NGC 3998
0056020701	12 00 48	-03 27 51	THIN	2.35	22.1	29.0	RXJ1200.8
0081340801	12 13 46	+02 48 41	THIN	1.78	17.8	22.3	IRAS12112
0056340101	12 19 23	+05 49 31	MEDIUM	1.56	22.0	27.5	NGC4261
0110990201	12 27 19	+01 29 24	THIN	1.85	7.9	9.7	HI1225+01
0124900101	12 31 32	+64 14 21	THIN	1.98	26.1	30.1	MS 1229.2+6430
0111550401	12 36 57	+62 13 30	THIN	1.51	75.4	87.1	HUBBLE DEEP
0110980201	12 45 09	-00 27 38	MEDIUM	1.73	46.3	55.5	NGC 4666
0136000101	13 04 12	+67 30 25	THIN	1.80	14.6	17.1	ABELL 1674
0056021001	13 08 33	+53 42 19	THIN	1.53	22.2	28.0	RX J1308.5
0111281601	13 41 24	-00 24 00	THIN	1.4	3.5	7.1	F864-7
0111281001	13 41 24	+00 24 00	THIN	1.0	5.8	10.0	F864-1
0111281401	13 43 00	+00 00 00	THIN	2.8	1.7	4.5	F864-5
0111282401	13 43 00	+00 24 00	THIN	2.0	3.0	6.6	F864-2
0111281701	13 43 24	-00 24 00	THIN	2.2	2.1	7.3	F864-8
0111281801	13 44 36	-00 24 00	THIN	3.6	—	7.7	F864-9
0111281501	13 44 36	+00 00 00	THIN	1.6	2.8	6.5	F864-6
0111282601	13 44 36	+00 24 00	THIN	2.0	2.2	7.7	F864-3
0112250201	13 47 41	58 12 42	MEDIUM	1.28	24.7	31.3	QSO 1345+584
0071340501	13 49 15	+60 11 26	THIN	1.80	14.1	18.1	NGC 5322
0112250101	13 54 17	-02 21 46	THIN	3.32	20.4	24.2	RXJ1354.3
0110930401	14 35 30	48 44 30	MEDIUM	2.08	—	7.0	NGC5689
0021540101	15 06 29	01 36 20	THIN	4.24	25.7	—	NGC 5846
0111260201	15 10 03	57 02 44	THIN	1.49	8.4	11.4	GB1508+5714

Table 1. The *XMM-Newton* pointings

Table 1 – *continued*

Obs ID	RA (J2000)	Dec (J2000)	FILTER	N_H (10^{20} cm^{-2})	PN exp. time (ksec)	MOS1 exp. time (ksec)	Field name
0145190201	15 15 54	56 19 44	THIN	1.44	19.4	28.6	NGC 5907
0103860601	15 16 40	00 14 54	THICK	4.67	8.9	13.2	CGCG21-63
0011830201	15 25 54	51 36 49	THIN	1.56	24.7	29.7	CSO 755
0150610301	15 36 38	54 33 33	THIN	1.32	16.0	24.3	PG 1535+547
0060370901	15 43 59	+53 59 04	THIN	1.27	14.2	19.2	SBS 1542+541
0025740401	16 04 19	43 04 33	THIN	1.25	12.5	15.7	CL1604+4304
0033540901	16 32 01	37 37 50	THIN	1.17	11.0	14.3	PG 1630+377
0107860301	17 01 23	+64 14 08	MEDIUM	2.65	2.3	3.9	RXJ 1701.3
0111180201	20 40 10	-00 52 16	MEDIUM	6.70	8.7	-	AE AQR
0093030201	21 29 38	00 05 38	MEDIUM	4.29	29.0	40.0	RXJ2129.6
0042341301	23 37 40	-00 16 33	THIN	3.82	8.2	13.3	RXCJ 2337.6+0016
0147580401	23 47 25	00 53 58	THIN	3.77	12.2	15.0	1AXGJ234725
0108460301	23 54 09	-10 24 00	MEDIUM	2.91	13.6	19.1	ABELL 2670

ID	α_X (J2000)	δ_X (J2000)	r (mag)	P (%)	δ_{XO} (arcsec)	f_x ($10^{-14} \text{ erg s}^{-1} \text{ cm}^{-2}$)	HR	$\log(f_x/f_o)$	z	$\log L_X$ (erg s^{-1})	type ¹
01	00 42 44.68	-09 33 16.27	15.20	0.01	1.1	1.41 ± 0.52	< -0.22	-2.38	0.054 ²	40.99	A
02	03 06 56.92	-00 00 24.41	17.71	0.16	2.5	0.32 ± 0.14	< -0.70	-2.02	0.109	40.99	C
03	03 25 31.40	-06 07 44.04	14.58	0.02	2.6	1.02 ± 0.47	< -0.13	-2.77	0.035 ²	40.46	E
04	03 58 05.25	+01 09 50.34	14.93	0.01	1.4	1.52 ± 0.34	-0.46 ± 0.28	-2.45	0.074 ³	41.30	A
05	08 30 59.81	+52 37 47.36	17.69	0.80	5.4	0.34 ± 0.12	-0.18 ± 0.84	-2.00	0.136	41.24	E
06	08 31 14.62	+52 42 25.32	15.24	0.01	0.9	0.56 ± 0.09	-0.79 ± 0.19	-2.76	0.064	40.74	C
08	08 32 02.52	+52 47 12.90	16.01	0.01	1.0	0.25 ± 0.08	$< +0.60$	-2.81	0.105 ³	40.84	E
09	08 32 28.21	+52 36 22.74	13.82	< 0.01	0.7	6.43 ± 0.28	< -0.99	-2.27	0.017	40.65	E
10	09 17 58.41	+51 51 08.91	16.68	0.33	4.6	0.61 ± 0.26	$< +0.07$	-2.15	0.219 ^{2,3}	41.92	A
11	09 35 18.92	+61 28 34.43	16.50	0.27	4.7	0.95 ± 0.24	-0.37 ± 0.28	-2.03	0.124	41.58	E*
12	09 36 19.41	+61 27 20.85	16.55	0.05	2.3	0.95 ± 0.21	< -0.41	-2.01	0.131	41.65	A
13	10 08 15.98	+53 42 15.19	16.71	0.08	2.3	0.73 ± 0.21	< -0.07	-2.06	0.069	40.93	E
14	10 23 06.49	+04 08 04.34	15.62	0.18	4.5	0.29 ± 0.14	$< +0.50$	-2.89	0.048	40.20	C
16	11 23 05.25	+05 38 40.42	15.02	< 0.01	0.3	1.28 ± 0.24	< -0.25	-2.49	0.049	40.86	E
17	11 28 45.85	+58 35 36.53	14.96	0.15	5.6	1.35 ± 0.32	-0.38 ± 0.60	-2.49	0.059	41.05	E*
18	11 50 32.52	+55 03 28.76	14.39	< 0.01	1.0	1.52 ± 0.20	-0.62 ± 0.19	-2.67	0.019 ²	40.14	C*
19	11 50 51.05	+55 08 37.14	13.52	< 0.01	1.9	1.03 ± 0.26	-0.38 ± 0.26	-3.19	0.019 ²	39.93	C*
20	12 19 35.76	+05 50 48.30	12.67	< 0.01	2.6	1.29 ± 0.24	-0.80 ± 0.26	-3.43	0.008 ²	39.26	A
21	12 31 46.84	+64 14 03.34	13.01	< 0.01	3.0	1.95 ± 0.14	-0.38 ± 0.13	-3.11	0.002	38.39	A
22	12 32 53.11	+64 08 56.02	15.43	0.17	5.1	1.03 ± 0.26	< -0.26	-2.42	0.140 ³	41.72	E
23	12 44 52.21	-00 25 50.70	15.34	0.01	1.3	0.56 ± 0.11	< -0.34	-2.72	0.082	40.97	C
24	12 45 32.14	-00 32 05.01	13.12	0.01	4.2	2.83 ± 0.19	-0.45 ± 0.09	-2.91	0.005	39.29	E
25	13 03 01.51	+67 25 20.73	16.16	0.16	3.7	1.38 ± 0.34	< -0.28	-2.00	0.109 ^{2,3}	41.62	A
26	15 07 07.69	+01 32 39.26	11.65	< 0.01	2.5	3.30 ± 0.37	-0.69 ± 0.11	-3.43	0.009	39.83	A
27	15 09 46.77	+57 00 00.76	11.68	< 0.01	1.7	6.75 ± 0.52	-0.27 ± 0.10	-3.11	0.003	39.18	A
29	21 29 33.97	+00 01 35.97	16.12	0.01	1.0	0.35 ± 0.23	$< +0.05$	-2.61	0.052	40.35	A
30	23 53 40.52	-10 24 17.79	15.07	0.02	2.1	2.52 ± 0.51	< -0.62	-2.18	0.074 ²	41.52	A
31	23 54 05.71	-10 18 33.07	15.70	0.05	2.5	1.06 ± 0.33	< -0.06	-2.30	0.073 ²	41.14	A

¹ A: absorption lines; E: Narrow emission lines; C: both narrow emission and absorption lines. The * denotes ambiguous SDSS spectral classification.² source at the same redshift as the target of the *XMM-Newton* pointing.³ Photometric redshift from the SDSS.

The columns are: 1: identification number; 2,3: right ascension and declination of the X-ray source (J2000); 4: optical magnitude;

5: probability the optical counterpart is a spurious alignment; 6: X-ray/optical position offset;

7: absorbed X-ray flux in the 0.5–8 keV spectral band in units of $10^{-14} \text{ erg s}^{-1} \text{ cm}^{-2}$;

8: Hardness ratio derived in the 0.5–2 and 2–8 keV bands; 9: X-ray-to-optical flux ratio; 10: spectroscopic or photometric redshift from the SDSS;

11: Logarithmic 0.5–8 keV X-ray luminosity in units of $10^{41} \text{ erg s}^{-1}$; 12: spectral type.**Table 2.** The candidate ‘normal’ galaxy sample.

al. (2004). From Fig. 2 it can be seen that our sample is complementary to the CDF, covering the low redshift and high luminosity part of the luminosity-redshift plane.

We derive the binned ‘normal’ galaxy X-ray luminosity function using the method described by Page & Carrera (2000). This is variant of the classical non-parametric $1/V_{max}$ method (Schmidt 1968) and has the advantage that it is least affected by systematic errors for objects close to the flux limit of the survey. For a given redshift and X-ray

luminosity interval the binned luminosity function is estimated from the relation:

$$\Phi(L) = \frac{N}{\int_{L_{min}}^{L_{max}} \int_{z_{min}(L)}^{z_{max}(L)} \Omega(L, z) dV/dz dz dL}, \quad (2)$$

where N is the number of sources with luminosity in the range L_{min} and L_{max} and dV/dz is the volume element per redshift interval dz . For a given luminosity L , $z_{min}(L)$ and $z_{max}(L)$ are the minimum and the maximum redshifts

ID	α_X (J2000)	δ_X (J2000)	r (mag)	P (%)	δ_{XO} (arcsec)	f_x (10^{-14} cgs)	HR	$\log(f_x/f_o)$	z	$\log L_X$ (erg s^{-1})	type ¹
07	08 31 39.11	+52 42 06.87	15.70	0.02	1.4	2.07 ± 0.14	$+0.50 \pm 0.07$	-2.01	0.059	41.23	E
15	10 52 47.89	+57 36 20.56	17.98	0.13	2.2	0.20 ± 0.09	$+0.22 \pm 0.62$	-2.10	0.118	40.87	E
28	15 16 27.00	+00 23 03.30	15.78	0.01	1.1	1.63 ± 0.56	$+0.20 \pm 0.34$	-2.08	0.053 ²	41.04	A

¹A: absorption lines; E: Narrow emission lines; C: both narrow emission and absorption lines.

²source at the same redshift as the target of the *XMM-Newton* pointing.

Columns as in table 2

Table 3. The excluded hard Low Luminosity AGN.

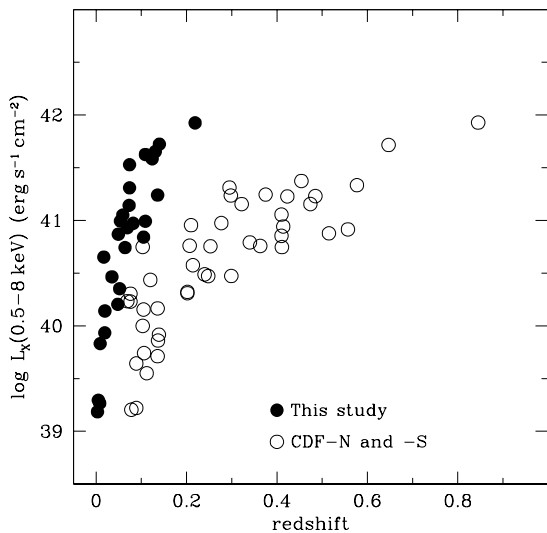


Figure 2. L_X (0.5 – 8 keV) against redshift. Filled circles are for our sample of ‘normal’ galaxy candidates (including sources associated with the prime target of a given *XMM-Newton* pointing). Open circles represent the CDF samples. The NHS and CDF surveys cover complementary regions of the L_X – z space.

possible for a source of that luminosity to remain within the flux limits of the survey and to lie within the redshift bin. $\Omega(L, z)$ is the solid angle of the X-ray survey available to a source with luminosity L at a redshift z (corresponding to a given flux in the X-ray area curve). The logarithmic bin size of the luminosity function varies so that each bin comprises approximately equal number of sources N . The uncertainty of a given luminosity bin is estimated assuming Poisson statistics from the relation:

$$\delta\Phi(L) = \frac{\sqrt{N}}{\int_{L_{min}}^{L_{max}} \int_{z_{min}(L)}^{z_{max}(L)} \Omega(L, z) \left(\frac{dV}{dz}\right) dz dL}. \quad (3)$$

We also derive the luminosity function using the parametric Maximum Likelihood Method (ML; Tammann, Yahil & Sandage 1979). We use a Schechter (1976) form for the luminosity function as this describes very well the luminosity function in e.g. optical wavelengths (Bingelli, Sandage & Tammann 1988). Moreover, it has a strong theoretical footing as it is derived from self-similar gravitational collapse models (Press & Schechter 1974). The Schechter function is expressed as:

$$\Phi(L) = \phi_*(L/L_*)^{-\alpha} \exp(-L/L_*) dL. \quad (4)$$

In the above expression L_* denotes the characteristic luminosity where the function above changes from a power-law with slope α at the faint-end to an exponential drop at brighter luminosities. A likelihood function is constructed as the product of probabilities P_i that a galaxy at redshift z is detected with a luminosity L . Thus P_i is defined as the ratio of the number of galaxies with luminosity between L and $L + dL$ over the total number observed, $P_i = \Phi(L)/\int_{L_{min}(z)}^{\infty} \Phi(L) dL$. Then we maximise the sum $\sum_n \ln P_i$ by varying L_* and α . The errors on L_* and α are estimated from the $\delta L = 0.5$ regions around the maximum likelihood fit. Since the normalization ϕ_* of the luminosity function cancels out in the calculation above, we derive ϕ_* from

$$\phi_* = N_{gal} / \int \int \Omega(L, z) \Phi(L) / \phi_* dL dV/dz dz \quad (5)$$

where N_{gal} is the total number of galaxies in the survey and $\Omega(L, z)$ is the solid angle of the X-ray survey available to a source with luminosity L at a redshift z , i.e. the area curve at different flux limits. The uncertainty in ϕ_* is approximated by performing 200 bootstrap resamples of the data and then estimating the 25th and 75th quartile around the median. For a Gaussian distribution these correspond to the 68 per cent confidence level.

We improve the statistical reliability of our luminosity function estimates by combining our sample with 18 $z < 0.22$ galaxies from the CDF-N and CDF-S. As already discussed the CDF-N data are obtained from Hornschemeier et al. (2003) by selecting a total of 10 sources with 0.5-8 keV band detection. All of these systems have spectroscopic redshifts available. In the case of the CDF-S we select a total of 8 sources detected in the 0.5-2.0 keV spectral band with $\log(f_x/f_o) < -2$ from the catalogue presented by Giacconi et al. (2002). Spectroscopic (total of 5) or photometric (total of 3) redshifts are available from Szokoly et al. (2004) and Zheng et al. (2004) respectively.

We estimate the luminosity function using the methods discussed above for 3 different subsamples: (i) the NHS data alone, i.e. without combining our sample with the CDF galaxies, (ii) both the NHS and the CDF galaxies and (iii) combined NHS and CDF data after excluding systems from our survey that are associated with the prime target of a given *XMM-Newton* pointing. The latter subsample is referred to as the ‘restricted sample’ and allows us to explore the sensitivity of our results to the presence of group or cluster members within the NHS. Figure 3 plots the local luminosity function for the subsamples (ii) and (iii). For clarity we do not show the luminosity function for sample (i). We

find that the luminosity function for the restricted sample very closely resembles that of the total sample. Henceforth, we will be using the total sample (ii) in our analysis.

The luminosity function derived above contains all galaxy types i.e. both early and late. Next, we attempt to explore the luminosity function for different galaxy types using the combined NHS/CDF sample. Galaxies with absorption optical lines are classified as early while systems with narrow emission-lines or galaxies presenting both absorption and emission lines are grouped into the late type category. For systems without optical spectra we use the best-fit SED estimated as a by-product of the photometric redshift estimation for classification. There are 27 and 19 late and early type galaxies respectively. The results are shown in Fig. 4 and are compared with the predicted star-forming X-ray galaxy luminosity function derived by Georgantopoulos, Basilakos & Plionis (1999). This is estimated by convolving the optical star-forming luminosity function with the optical-to-X-ray luminosity relation. The optical luminosity function has been derived from the Ho et al. (1997) spectroscopic sample of galaxies whereas the optical-to-X-ray luminosity relation is taken from the *Einstein* sample of Fabbiano et al. (1992). We also plot the X-ray luminosity function derived by Norman et al. (2004) by convolving the 'warm' IRAS luminosity function (Takeuchi et al. 2003) with the X-ray-to-far-infrared luminosity relation for star-forming galaxies (Ranalli et al. 2003).

In Table 4 we summarise the best-fit parameters for the slope and the break luminosity as well as the normalization derived from the maximum likelihood method. In the same table we give the X-ray emissivity (luminosity per Mpc^3)

$$j_x = \int \Phi(L) L dL, \quad (6)$$

as well as the fractional contribution to the 0.5-8 keV X-ray background. The integrated galaxy X-ray flux is given by

$$I = \frac{c}{4\pi H_0} \int_{z_1}^{z_2} \frac{j_x (1+z)^{p-\alpha_x}}{(1+z)(\Omega_m (1+z)^3 + \Omega_\Lambda)^{1/2}} dz. \quad (7)$$

We integrate all luminosities from $10^{38} \text{ erg s}^{-1}$ to infinity up to a maximum redshift of $z = 2$. We have assumed an energy spectral index of $\alpha_x = 0.7$ (e.g. Zelaz, Georgantopoulos & Ward 1998). The X-ray background intensity in the 0.5-8 keV band is taken from Gendreau et al. (1995). The X-ray flux sensitively depends on the assumed form of galaxy evolution. Hopkins (2004) combined the luminosity function information at many wavelengths, from radio to X-rays and concluded that the luminosity density evolves as $(1+z)^p$ with $p = 3.3$ for $z < 1$, while for higher redshifts it appears to remain constant. Norman et al. (2004) find a luminosity evolution consistent with $p=2.7$ at X-ray wavelengths up to their maximum redshift of $z \approx 1$, close to the value derived by Hopkins (2004). In Table 4, we give the contribution to the X-ray background (I/I_{XRB}) for both evolution indices. The errors for both j_x and I/I_{XRB} are estimated in the same manner as the uncertainties in ϕ_* .

5 DISCUSSION

We use a total of 70 *XMM-Newton* fields overlapping with the SDSS-DR2 to compile a sample of 28 X-ray selected

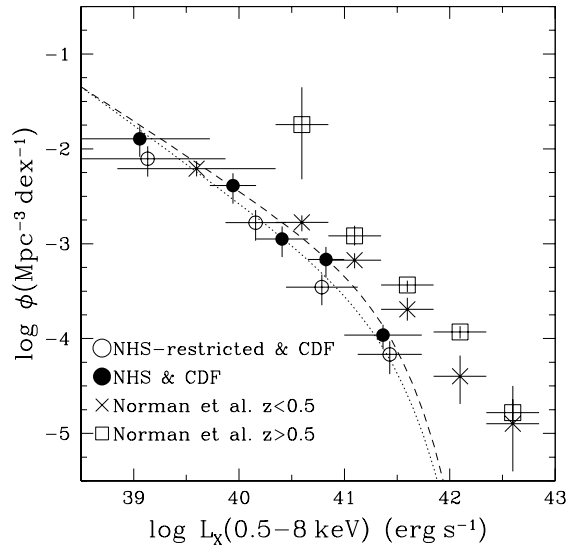


Figure 3. The local luminosity function derived using the non-parametric method for the combined NHS/CDF sample is denoted with filled (open) circles in the case where we keep (exclude) the galaxies associated with the target. The dashed and dotted lines correspond to the maximum likelihood determination in the above two cases (NHS-restricted/CDF and NHS-total/CDF respectively). The luminosity function derived by Norman et al. (2004) in two redshift bins is plotted for comparison.

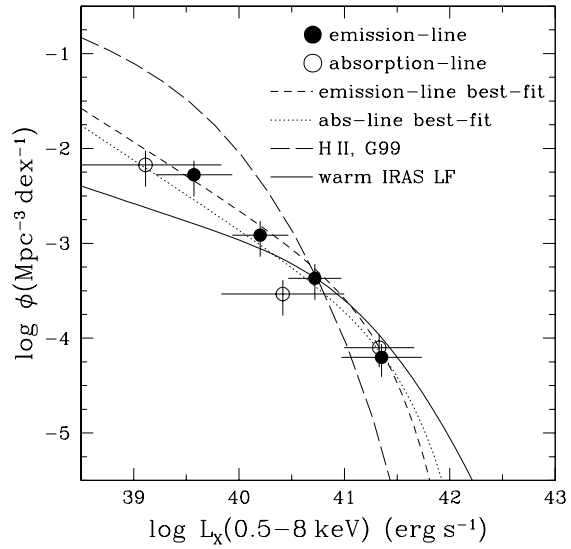


Figure 4. The luminosity function derived using the non-parametric method in the case of the emission (filled circles) and absorption line (open circles) galaxies. The short-dashed and dotted lines give the corresponding maximum likelihood Schechter form to these. The long-dashed line represents the local $\phi(L_X)$ estimated indirectly from the optical star-forming galaxy luminosity function (Georgantopoulos et al. 1999). The solid line corresponds to the $\phi(L_X)$ derived from the 'warm' IRAS galaxy luminosity function of Takeuchi et al. (2003).

Sample	$\log L_\star^1$	α	ϕ_\star^2	j_x^3	I/I_{XRB}^4	I/I_{XRB}^5
NHS	$41.38^{+0.23}_{-0.18}$	$1.86^{+0.30}_{-0.29}$	$3.40^{+1.61}_{-1.82}$	$1.52^{+0.16}_{-0.09}$	$0.17^{+0.05}_{-0.05}$	$0.12^{+0.02}_{-0.02}$
NHS/CDF	$41.46^{+0.18}_{-0.15}$	$1.78^{+0.12}_{-0.12}$	$2.54^{+3.13}_{-0.82}$	$1.07^{+0.06}_{-0.07}$	$0.15^{+0.01}_{-0.01}$	$0.11^{+0.01}_{-0.01}$
NHS/CDF restricted	$41.28^{+0.21}_{-0.26}$	$1.80^{+0.16}_{-0.18}$	$3.01^{+2.3}_{-1.8}$	$0.89^{+0.08}_{-0.04}$	$0.11^{+0.01}_{-0.01}$	$0.08^{+0.01}_{-0.005}$
Emission	$41.23^{+0.22}_{-0.17}$	$1.71^{+0.17}_{-0.19}$	$3.3^{+2.81}_{-2.19}$	$0.65^{+0.04}_{-0.03}$	$0.09^{+0.01}_{-0.01}$	$0.06^{+0.004}_{-0.004}$
Absorption	$41.68^{+0.33}_{-0.25}$	$1.81^{+0.16}_{-0.19}$	$0.58^{+0.88}_{-0.51}$	$0.45^{+0.03}_{-0.03}$	$0.06^{+0.004}_{-0.004}$	$0.04^{+0.003}_{-0.003}$

¹ in units erg s^{-1} ; ² in units $\times 10^{-4} \text{Mpc}^{-3} \text{ dex}^{-1}$; ³ in units $\times 10^{38} \text{erg s}^{-1} \text{ Mpc}^{-3}$

⁴ evolution index $p=3.3$; ⁵ $p=2.7$

Table 4. The luminosity function best-fit parameters

‘normal’ galaxies with $z < 0.22$. These systems have X-ray-to-optical flux ratios ($\log(f_x/f_o) < -2$), luminosities ($L_X < 10^{42} \text{erg s}^{-1}$), X-ray colours and optical spectroscopic properties (available for most of our sources) all suggesting X-ray emission dominated by stellar processes (hot gas and X-ray binaries) rather than accretion on a supermassive black hole. Using this carefully selected sample we construct the local ($z \lesssim 0.2$) X-ray luminosity function of ‘normal’ galaxies. Our *XMM-Newton* survey nicely complements the deeper *Chandra* surveys in the coverage of the $L_X - z$ plane probing lower redshifts and higher luminosities. We combine the two samples, exploiting the depth of *Chandra* and the wide areal coverage of the NHS, to provide a ‘normal’ galaxy sample totaling 46 systems at $z < 0.22$.

We attempt to assess the efficiency of the $\log(f_x/f_o) < -2$ criterion in selecting the most luminous normal galaxies. We use the star-forming galaxy sample compiled by Zezas (2001) which comprises *ROSAT* PSPC observations of systems classified on the basis of high quality nuclear spectra from Ho et al. (1997). The above sample comprises 43 galaxies, detected by PSPC either as targets or serendipitously, spanning the luminosity range $L_X(0.1 - 2.4 \text{keV}) \approx 4 \times 10^{37} - 3 \times 10^{41} \text{erg s}^{-1}$. We estimate the $\log(f_x/f_o)$ ratio from the 0.1-2.4 keV flux and the *B*-band magnitude. We find that no galaxy lies above the $\log(f_x/f_o) = -2$ cut, despite the fact that highly luminous galaxies are included in the sample. Nevertheless, we note that the most X-ray luminous ($\approx 2 \times 10^{42} \text{erg s}^{-1}$) star-forming system known, NGC3256 (Moran, Lehnert & Helfand 1999), which is not included in the Ho et al. (1997) sample, has a relatively high X-ray-to-optical flux ratio, $\log(f_x/f_o) \approx -1.7$. This suggests that some very X-ray luminous galaxies would evade our $\log(f_x/f_o) < -2$ criterion. This effect may be exacerbated at higher redshift. Indeed, in a scenario where the $\log(f_x/f_o)$ increases with redshift (Hornschemeier et al. 2003), the fraction of missed galaxies will be higher.

We further attempt to estimate the contamination of our sample by Low Luminosity AGN. We use the late-type galaxy sample of Shapley et al. (2001) comprising a total of 101 systems with $\log(f_x/f_o) < -2$. A number of these are classified AGNs, primarily using information from the optical spectra obtained by Ho et al. (1997). Note that we include only the Seyfert and Liner1.9 objects in the AGN class. We find 15 such objects which satisfy the above criteria and this roughly translates to ~ 15 per cent contamination in the Shapley et al. sample. This may only represent a lower limit as not all galaxies in Shapley et al. are common with Ho et al. (1997) i.e. many systems do not have good quality spectra. We note nevertheless, that even in the case

where a small fraction of residual Low Luminosity AGN is included in our sample (because of the quality of the optical spectra), this does not necessarily mean that the X-ray emission comes only from the AGN in these objects, e.g. Terashima & Wilson (2003).

The X-ray luminosity function of the combined sample with a median redshift $z_{median} = 0.076$ is compared in Figure 3 with the results at higher- z of Norman et al. (2004). These authors derived the first ever X-ray galaxy luminosity function, using data from the combined CDF-North and South. Their sample probing redshifts up to $z \approx 1$ is split into two redshift bins with median $z = 0.26$ and $z = 0.66$ respectively. Inspection of Fig. 3 shows that their ‘quasi-local’ $z < 0.5$ luminosity function is in good agreement with ours especially at the faint end. At bright luminosities the CDF luminosity function is significantly higher than ours. This may suggest contamination of the Norman et al. (2004) sample by AGNs at bright luminosities. This is not highly unlikely, especially at luminosities brighter than $10^{42} \text{erg s}^{-1}$, since there is no optical spectroscopy available for all the sources of Norman et al. (2004). Alternatively, we may be witnessing evolution of the ‘normal’ galaxy luminosity function. The median redshift of the $z < 0.5$ subsample of Norman et al. is $z_{median} = 0.26$ higher than our median redshift $z = 0.076$. For luminosity evolution of the form $(1+z)^{2.7}$ derived by Norman et al. (2004), a source at $z = 0.26$ is expected to become 1.5 times more luminous relative to $z = 0.076$. Moreover, we are excluding from our analysis systems with X-ray to optical flux ratio $\log(f_x/f_o) > -2$ and therefore, our sample may be biased against X-ray ultra-luminous star-forming galaxies, especially those with $L_X \gtrsim 10^{42} \text{erg s}^{-1}$ (see e.g. Moran et al. 1999). Norman et al. (2004) use the log-norm functional form for fitting their luminosity function. We note that such a form describes equally well our data; the fit yields $\Delta L \approx 1.4$ relative to the Schechter best-fit, which can be considered however as only a marginal improvement as the log-norm functional form has an additional free parameter. In any case, the statistics are still limited and a detailed comparison of the Schechter and log-norm functional forms has to await till more data are accumulated.

The luminosity function derived above encompasses both late and early galaxy types. Figure 4 presents the $\phi(L_X)$ estimates for these two classes separately. These are compared with the local X-ray luminosity functions derived from (i) optically selected star-forming galaxies (Georgantopoulos et al. 1999) and (ii) warm IRAS galaxies (Norman et al. 2004). The former largely overestimates the number of emission-line systems at low luminosities while the lat-

ter provides a better representation of the X-ray luminosity function although it underpredicts the number of galaxies with $L < L_*$.

The optical luminosity function of early and late type galaxies has been derived by Madgwick et al. (2002) using a total of 75,000 galaxies from the 2dF Galaxy Redshift Survey classified according to their spectral properties. Four spectral types are defined ranging from passive absorption line systems (earliest type) to actively star-forming galaxies (latest type). Madgwick et al. (2002) find that the luminosity function of all four classes is well represented by a Schechter form with comparable M_\star^B (within 0.4 mag) and slopes that are getting steeper from early to late-type galaxies (α ranging from 0.54 to 1.5). Interestingly, at X-ray wavelengths, the luminosity functions we derive for early and late type systems are comparable in both their shapes and normalizations, at odds with the results from the optical regime. For example we note that the slope of the X-ray luminosity function should be flatter than that at optical wavelengths for an X-ray-to-optical luminosity relation steeper than linear (e.g. $L_X \propto L_B^{1.8}$; Fabbiano et al. 1992). Larger samples than the one used here are required to further explore this issue.

Using the X-ray luminosity functions derived above we can provide the most accurate yet estimates of the local galaxy X-ray emissivity (Table 4). In the 0.5-8 keV band this is estimated to be $\approx 10^{38} \text{ erg s}^{-1} \text{ Mpc}^{-3}$ with about equal contributions from early and late type systems. The emissivities derived here are somewhat lower but still consistent within the uncertainties with those estimated by Georgakakis et al. (2004a) via stacking analysis of 2dF galaxies. Furthermore, adopting the star-formation rate evolution model of Hopkins (2004) and Norman et al. (2004) we estimate the contribution of galaxies to the X-ray background. This amounts to about 10-20 per cent for all galaxies, up to a maximum redshift of $z = 2$ with the evolution truncated at $z = 1$. The exact fraction depends on the evolution index used and the sample used. If we assume that the luminosity evolution continues up to $z=2$ we obtain contributions which are higher by about a factor of two. We find a contribution to the X-ray background of 9 and 6 per cent for emission and absorption line galaxies respectively using the $p=3.3$ evolution model truncated at $z = 1$. However, it is possible that the absorption line systems, associated with early-type galaxies, do not present such strong evolution with cosmic time (Lilly et al. 1995). Assuming no evolution for these systems we assess that they contribute about 2 per cent to the XRB. The fractions derived above are higher than those in the CDF-North. For example Hornschemeier et al. (2003) estimate that 1-2 per cent of the 0.5-2 keV XRB could arise in normal galaxies. However, this is estimated by adding the fluxes of optically selected galaxies in the CDF-North survey and therefore should be considered as a lower limit as it does not take into account the contribution of optically fainter systems.

6 CONCLUDING REMARKS

The *Chandra* and *XMM-Newton* missions opened a new window in the study of distant galaxies by providing the first X-ray selected normal galaxy sample. *XMM-Newton* owing

to its large field-of-view can constrain efficiently the local ($z \lesssim 0.2$) X-ray galaxy luminosity function. The *Chandra* deep fields probe normal galaxies with a median redshift of $z \approx 0.3$ (up to a maximum redshift of $z=1$) yielding information on the evolution of the galaxies at X-ray wavelengths. However, the peak of the star-formation activity lies at even higher redshifts which remain beyond the reach of the current X-ray missions. These distant galaxies reside at fluxes fainter than $10^{-17} \text{ erg cm}^{-2} \text{ s}^{-1}$. This flux regime can be accessed, and thus the study of galaxies at X-ray wavelengths will only be furthered, with the launch of high effective area missions ($> 30 \text{ m}^2$) combined with excellent positional accuracy ($< 2 \text{ arcsec}$ necessary to minimize confusion problems) such as the European Space Agency's mission *XEUS*.

7 ACKNOWLEDGMENTS

We are grateful to the anonymous referee for his/her suggestions which helped to improve substantially this paper. This work is jointly funded by the European Union and the Greek Ministry of Development in the framework of the programme 'Promotion of Excellence in Technological Development and Research', project 'X-ray Astrophysics with ESA's mission XMM'. We also acknowledge support from the Greek General Secretariat for Research and Technology programme 'Exploring galaxies with NASA's *Chandra* X-ray mission'. We acknowledge the use of data from the *XMM-Newton* Science Archive at VILSPA.

Funding for the creation and distribution of the SDSS Archive has been provided by the Alfred P. Sloan Foundation, the Participating Institutions, the National Aeronautics and Space Administration, the National Science Foundation, the U.S. Department of Energy, the Japanese Monbukagakusho, and the Max Planck Society. The SDSS Web site is <http://www.sdss.org/>. The SDSS is managed by the Astrophysical Research Consortium (ARC) for the Participating Institutions. The Participating Institutions are The University of Chicago, Fermilab, the Institute for Advanced Study, the Japan Participation Group, The Johns Hopkins University, Los Alamos National Laboratory, the Max-Planck-Institute for Astronomy (MPIA), the Max-Planck-Institute for Astrophysics (MPA), New Mexico State University, University of Pittsburgh, Princeton University, the United States Naval Observatory, and the University of Washington.

REFERENCES

- Alexander D., et al., 2003, AJ, 126, 539
- Bingelli, B., Sandage, A., Tammann, G.A., 1988, ARA&A, 26, 509
- Dickey, J.M., & Lockman, F.J., 1990, ARA&A 28, 215
- Downes A. J. B., Peacock J. A., Savage A., Carrie D. R., 1986, MNRAS, 218, 31
- Fabbiano, G. 1989, ARA&A, 27, 87
- Fabbiano, G., Kim, D.W., Trinchieri, G., 1992, ApJS, 80, 531
- Fukugita M., Ichikawa T., Gunn J. E., Doi M., Shimasaku K., Schneider D. P., 1996, AJ, 111, 1748
- Gendreau, K. et al. 1995, PASJ, 47, L5
- Georgakakis A., et al., 2004a, MNRAS, 349, 135

Georgakakis, A.E., Georgantopoulos, I., Basilakos, S., Plonis, M., Kolokotronis, V., 2004b, MNRAS, 354, 123

Georgantopoulos I., Basilakos S., Plonis M., 1999, MNRAS, 305, L31.

Giacconi R., et al., 2002, ApJS, 139, 369

Gilfanov, M., Grimm, H.J., Sunyaev, R., 2004, MNRAS, 347, L57

Ho L. C., Filippenko A. V., Sargent W., 1997, ApJS, 112, 315.

Hopkins, A., 2004, ApJ, 615, 209

Hornschemeier A. E., Brandt W. N., Alexander D. M., Bauer F. E., Garmire G. P., Schneider D. P., Bautz M. W., Chartas G., 2002, ApJ, 568, 82

Hornschemeier A. E. et al., 2003, AJ, 126, 575

Kilgard, R. E., Kaaret, P., Krauss, M.I., Prestwich, A.H., Raley, M.T., Zezas, A., 2002, ApJ, 573, 138

Lilly, S.J., Tresse, L., Hammer, F., Crampton, D., Le Fevre, O., 1995, ApJ, 455, 108

Madgwick, D.S. et al. 2002, MNRAS, 333, 133

Manners, J.C. et al., 2003, MNRAS, 343, 293

Miller, C.J., Nichol, R.C., Gmez, P.L., Hopkins, A.M., Bernardi, M., 2003, ApJ, 597, 142

Moran, E.C., Lehnert, M.D., Helfand, D.J. 1999, ApJ, 526, 649

Norman C., et al., 2004, ApJ, 607, 721

Page, M.J. & Carrera, F.J. 2000, MNRAS, 311, 433

Press, W.H., Schechter, P., 1974, ApJ, 187, 425

Ranalli, P., Comastri, A., Setti, G., 2003, A&A, 399, 39

Read A. M., Strickland D. K., Ponman T. J., 1997, MNRAS, 286, 626.

Schechter, P., 1976, ApJ, 203, 297

Schmidt, M. 1968, ApJ, 151, 393

Shapley, A., Fabbiano, G., Eskridge, P.B., 2001, ApJS, 137, 139

Stevens I. R., Read A. M., Bravo-Guerrero J., 2003, MNRAS, 343, L47

Stocke, J. T. et al., 1991, ApJS, 76, 813

Stoughton C., et al., 2002, AJ, 123, 485.

Strüder L., Briel U., Dennerl K., et al. 2001, A&A, 365, L18.

Szokoly, G.P., et al., 2004, ApJS, 155, 271

Tajer, M., Trinchieri, G., Wolter, A., Campana, S., Moretti, A., Tagliaferri, G., A&A, in press, astro-ph/0412588

Takeuchi, T.T., Yoshikawa, K.I., Takako T., 2003, ApJ, 587, L89

Tammann, G.A., Yahil, A., Sandage, A., 1979, ApJ, 234, 775

Terashima, Y., & Wilson, A.S., 2003, ApJ, 583, 145

Turner M. J. L., Abbey A., Arnaud M., et al., 2001, A&A, 365, L27.

York D. G., et al., 2000, AJ, 120, 1579.

Zezas, A., Georgantopoulos, I., Ward, M.J., 1998, MNRAS, 301, 915

Zezas, A., 2001, Ph.D. Thesis, Univ. of Leicester

Zheng, W. et al. 2004, ApJS, 155, 73